



Bridging the Gap Between Applied Meteorology and Climate Science: A White Roof Example

Dan Li *^{1,2}

¹Department of Earth and Environment, Boston University, Boston, USA

²Department of Mechanical Engineering, Boston University, Boston, USA

Abstract

White roof is a widely-studied urban heat mitigation strategy and frequently incorporated into climate adaptation plans by cities. Assessing the effects of white roofs on temperature has often been approached from the perspective of applied meteorology. Here, the white roof problem is reframed as a climate science problem by focusing on the roof surface temperature, incorporating concepts of climate forcing, sensitivity, and feedback, and utilizing a linearized surface energy balance (SEB) model. Different from the Albedo Cooling Effectiveness (ACE) index used for *quantifying* white roof effects, a new index called Albedo Cooling Sensitivity (ACS_s , where the subscript ‘s’ indicates surface) is proposed as a stepping stone towards *understanding* white roof effects. The variability of ACS_s simulated by the Weather Research and Forecasting (WRF) model is found to be strongly related to the variability of convective heat transfer efficiency. It is recommended that climate forcing, sensitivity, and feedback be systematically integrated into the analysis of diverse urban adaptation strategies.

Keywords: Urban Heat Mitigation, White Roof, Albedo Cooling Effectiveness, Albedo Cooling Sensitivity

1 Introduction

Urban meteorology and climatology are often viewed as a branch of applied meteorology and climatology [20]. According to [2], applied climatology covers four basic areas: 1) design of structures and planning of activities; 2) assessments of current and past conditions, including

*Corresponding Author

E-mail address: lidan@bu.edu

doi: <https://doi.org/10.5149/ARC-GR.1418>

This work is licensed under a [Creative Commons “Attribution-NonCommercial 4.0 International”](https://creativecommons.org/licenses/by-nc/4.0/) license.



29 evaluation of extreme events; 3) study of the relationships between weather/climate condi-
30 tions and those in other parts of the physical and socioeconomic worlds; and 4) operation
31 of weather-sensitive systems that employ climatic information in making decisions. Clearly,
32 urban climatology fits into this scope. For example, urban meteorological and climate infor-
33 mation is pivotal for the design of buildings and other infrastructure in cities.

34 As urban populations grow and global temperatures rise, urban meteorology and climatol-
35 ogy are playing an increasingly crucial role in fostering more sustainable, resilient, and livable
36 cities. A case in point is climate adaptation, particularly in relation to heat mitigation. One
37 area of active research in urban meteorology and climatology is the assessment of the ef-
38 fectiveness of climate action plans using numerical modeling. This line of research has been
39 primarily approached from the perspective of applied meteorology, where the effects of various
40 adaptation strategies (on temperature and other environmental variables) are quantified for
41 studied cities and periods [e.g. 11].

42 The premise of this paper is that evaluating the effectiveness of climate action plans offers
43 not only opportunities to test and improve our simulation capabilities, but also new avenues
44 to enhance our understanding of urban climate processes. White roof, a widely studied heat
45 mitigation strategy, is used as an illustrative example.

46 2 Albedo Cooling Effectiveness (ACE)

47 2.1 Definition and Calculation

48 The basic physics of the white roof problem are straightforward: as the roof surface albedo
49 (α) is increased, more solar radiation is reflected and thus less is absorbed, leading to less
50 sensible heating of the near-surface air and less heat conduction into the roof deck and thus
51 building interior. A common theme in urban climate research over the last two decades
52 has been developing physically based modeling tools to simulate the urban environment,
53 based on which the white roof effects can be quantified. A highly successful model for such
54 purposes [3] is the so-called single-layer urban canopy model (SLUCM) [9], where an idealized
55 urban canyon consisting of roof, wall, and canyon floor (Figure 1a) is used to represent three-
56 dimensional, complex urban environments in coarse-resolution weather and climate models
57 (e.g., the Weather Research and Forecasting or WRF model [19]). Using this idealized canyon
58 representation of urban environment, white roofs can be readily simulated by increasing the
59 albedo of the roof facet (c.f., Figure 1c and 1a).

60 A typical study of SLUCM-enabled simulation of white roof effects is shown in Figure
61 2. Here the simulations are performed for the greater Boston area over a 5-day heatwave
62 event (July 20-24, 2022, with a spin-up day of July 19) using WRF (version 4.2.2). The
63 domain configurations and physical parameterizations follow a previous study [12], where
64 model validation can be also found. To quantify the white roof effects, two runs are performed:
65 a control run with the roof albedo of 0.2 (Figure 2a) and a high albedo run with the roof
66 albedo of 0.6 (Figure 2b). Here the simulated near-surface air temperature (represented by
67 the widely used 2-m air temperature T_2) in the domain with a spatial resolution of 1 km is
68 shown. Focusing on urban grid cells, the majority of urban land experiences lower T_2 in the
69 high albedo run (c.f., Figure 2b and 2a), as expected. However, in certain areas T_2 increases
70 in the high albedo run (more about this later). The difference between the high albedo run
71 and the control run in terms of T_2 (denoted as ΔT_2 , where Δ indicates the difference between
72 the high albedo run and the control run with the high albedo run minus the control run)
73 ranges from -0.6 to 0.2 K (Figure 2c).

74 An index called Albedo Cooling Effectiveness (ACE) is often used to quantify the effec-

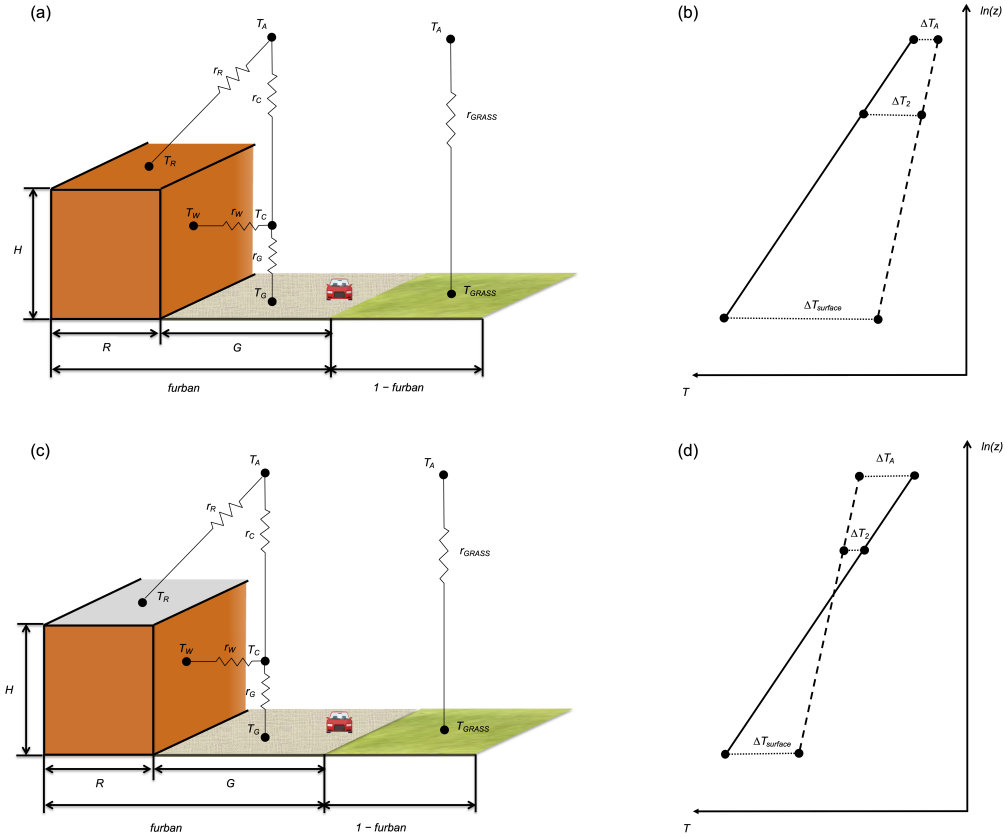


Figure 1: (a) A schematic of the SLUCM in WRF. For each grid cell that is classified as an urban grid cell, WRF-SLUCM treats the grid cell as a combination of an impervious part (with a fraction of f_{urban}) and a pervious grass part (with a fraction of $1 - f_{urban}$). In this figure, T is temperature and r is the resistance for heat transfer, and the subscripts A, R, W, C, G, GRASS represent atmosphere, roof, wall, canopy air, canyon ground, and grass, respectively. H , R , G represent the building height, the roof width, and the canyon width, respectively. (c) Similar to (a) but with white roof. (b) A schematic for changes (Δ) in temperatures due to white roofs. The solid line indicates the temperature profile without white roofs and the dashed line indicates the temperature profile with white roofs. White roofs lead to cooler surface temperature $T_{surface}$ of this entire grid cell, which further leads to cooler 2-m air temperature T_2 and atmospheric temperature T_A . Here it should be emphasized that $T_{surface}$ is an aggregated surface temperature of the entire grid cell, and is not an area-averaged surface temperature across all facets within this grid cell. (d) Similar to (b) except that the atmospheric temperature T_A is increased when white roofs are implemented, leading to increased 2-m air temperature T_2 . In (b, d), the temperature profile within the surface layer is assumed to be logarithmic for illustration purposes, although in reality the temperature profile is not always logarithmic. A change in the slope of the temperature profile due to white roofs indicates a change of atmospheric stability within the surface layer.

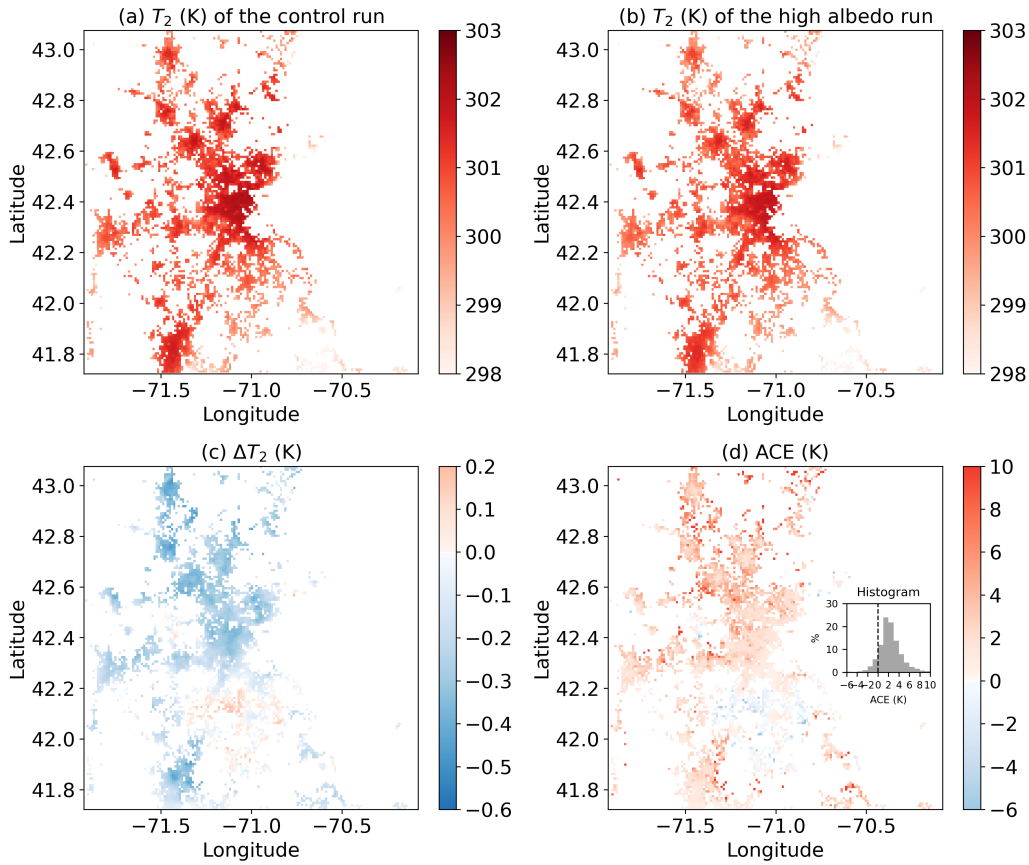


Figure 2: White roof effects on 2-m air temperature (T_2) over the greater Boston area simulated by WRF at a spatial resolution of 1 km (roughly corresponding to the neighborhood scale). (a) T_2 of the control run (K), (b) T_2 of the high albedo run (K), (c) ΔT_2 (K), (d) ACE (K). The inset in (d) shows the histogram of ACE. Only the results over urban grid cells are shown and the results are averaged over a 5-day period from July 20 to July 24, 2022.

75 tiveness of reflective materials [7, 8], defined as

$$76 \quad \text{ACE} = -\frac{\Delta T}{\Delta \alpha}, \quad (1)$$

77 where ΔT (K) is the change of neighbourhood scale (on the order of a few hundred meters
78 to a kilometer), near-surface air temperature due to the change in the neighbourhood scale
79 albedo ($\Delta \alpha$). The change in the neighbourhood scale albedo ($\Delta \alpha$) can be further expressed as
80 $\Delta \alpha = \Delta \alpha_s f_s$, where the subscript ‘s’ refers to the modified surface. Hence, $\Delta \alpha_s$ is the change
81 in albedo of the modified surface and f_s is the horizontal area of modified surface divided by
82 the horizontal area of the neighborhood. In the WRF results shown in Figure 2d, ACE is
83 computed as $-\Delta T_2 / (\Delta \alpha_R f_R)$, where the subscript ‘R’ indicates that the modified surface is
84 the roof with $\Delta \alpha_R = 0.6 - 0.2 = 0.4$. Note that within each grid cell, only a fraction of land
85 is the impervious land (i.e., f_{urban} in Figure 1a) and only a fraction of the impervious land is
86 roof (i.e., $R/(R + G)$ in Figure 1a). In these WRF simulations, the impervious land fraction
87 varies across the domain, resulting in spatially variable f_R .

88 The ACE values reported by different modeling studies in the literature range from 0 to
89 20 K, as summarized in a recent review [8]. Focusing on a sub-sample of 47 higher quality
90 modeling studies, the reported ACE values range from 2 to 6 K [8]. In the simulations shown
91 in Figure 2, the majority of ACE values ranges from -2 to 8 K, with a median ACE value of
92 2.2 K and a mean ACE value of 2.8 K. These median/mean ACE values are within the range
93 reported in previous studies [8].

94 2.2 Transferability and Interpretability

95 Intercomparing ACE values from different studies may lead to the mistaken perception that
96 ACE is a constant. To be clear, the ACE defined in Eq. 1 *cannot* be constant. At a minimum,
97 it must vary with incoming solar radiation (SW_{in}). A simple thought experiment suggests
98 that in regions with stronger solar radiation, the same amount of increase in roof albedo should
99 theoretically result in a greater reduction in air temperature, assuming all other factors remain
100 equal. This is also why seasonally averaged or wintertime ACE values tend to be lower than
101 those during the summer [8].

102 A complete understanding of the spatio-temporal variability of ACE remains elusive, which
103 poses a problem since, regardless of the indices used to quantify the effects of white roofs,
104 their utility relies on our ability to understand (and even predict) their variability across time
105 and space. Without this understanding, the results reported in the literature would have
106 limited value for reference and, as a result, limited transferability. Under such conditions, the
107 problem becomes strictly an applied one, requiring recalculation of the values of these indices
108 whenever study locations or periods change.

109 A more subtle issue is that ACE is often defined with near-surface air temperature, which
110 is notoriously difficult to model in urban environments. The 2-m air temperature (T_2) from
111 numerical models is widely used to represent the near-surface air temperature. However, its
112 interpretation over complex and tall urban canopies remains a challenge [17]. Even if we as-
113 sume that T_2 is the correct temperature to use in this context, changes in T_2 as the roof albedo
114 changes can be difficult to interpret. To demonstrate this, ΔT_2 in Figure 2c is decomposed
115 into contributions from changes in various factors including the roof surface temperature (T_R),
116 the atmospheric temperature above the urban canopy (T_A), the wall and ground surface tem-
117 peratures (T_B , T_G), the grass temperature in the same grid cell (T_{GRASS}), and heat transfer
118 resistances (see Figure 1 for the definitions of these temperatures and resistances), following
119 the decomposition method in an earlier study [12].

120 Here the decomposition is performed separately for grid cells with positive and negative
121 ΔT_2 values to highlight their differences and similarities. It can be seen that for both posi-

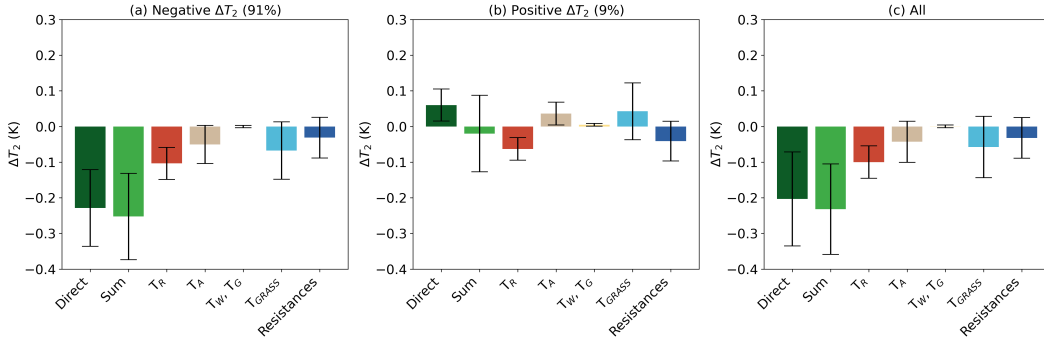


Figure 3: (a) The decomposition of ΔT_2 over urban grid cells with negative ΔT_2 values (91%), (b) The decomposition of ΔT_2 over urban grid cells with positive ΔT_2 values (9%), (c) The decomposition of ΔT_2 over all urban grid cells. The different bars represent, from left to right, computed ΔT_2 directly using WRF outputs, diagnosed ΔT_2 from the decomposition method, contribution from changes in the roof surface temperature (T_R), contribution from changes in the atmospheric temperature above the urban canopy (T_A), contribution from changes in the wall and ground surface temperatures (T_W , T_G), contribution from changes in the grass temperature in the same grid cell (T_{GRASS}), and contribution from changes in heat transfer resistances. The error bars are standard deviations that indicate spatial variability.

122 tive and negative ΔT_2 cases, contributions from the roof surface temperature are one of the
 123 most important contributions and are consistently negative, implying that the roof surface
 124 temperature is always reduced when the roof albedo is increased. This is not surprising given
 125 that the cooling signal originates from the roof surface. However, contributions from other
 126 factors such as the atmospheric temperature above the urban canopy, the grass temperature,
 127 and the heat transfer resistances are not negligible. For negative ΔT_2 cases (Figure 3a), the
 128 atmospheric temperature above the urban canopy is also reduced as the roof albedo increases
 129 (see Figure 1b for a schematic). However, for positive ΔT_2 cases (Figure 3b), the atmospheric
 130 temperature above the urban canopy is increased as the roof albedo increases (see Figure 1d
 131 for a schematic). Changes in the atmospheric temperature above the urban canopy are ex-
 132 tremely difficult to fully understand especially at the weather time scales, as these changes are
 133 strongly affected or even dominated by non-local atmospheric processes. In the simulations
 134 shown in Figure 2, it can only be conjectured that in certain regions warm advection causes
 135 the atmospheric temperature above the urban canopy (T_A) to increase even though the roof
 136 surface temperature (T_R) is reduced, leading to positive ΔT_2 and thus negative ACE values.

137 There is no reason why the effects of white roofs cannot be defined using other temperature
 138 metrics. In fact, a good candidate is the roof surface temperature (T_R), which can serve as
 139 an intermediate stepping stone. Intuitively, changes in roof albedo first cause the roof surface
 140 temperature to change (see Figure 4a, b), which then drive other changes such as near-surface
 141 air temperature, humidity, and wind fields. So the response of roof surface temperature to
 142 albedo increase is perhaps *easier* (but not necessarily easy) to understand. This argument is
 143 supported by the fact that changes in the roof surface temperature are always negative even
 144 in places where changes in T_2 are positive, as shown in Figure 4c. For comparison purposes,
 145 an ACE_s (Figure 4d) is defined based on the surface temperature and albedo changes of the
 146 modified surface, as follows

$$147 \quad ACE_s = -\frac{\Delta T_s}{\Delta \alpha_s}. \quad (2)$$

148 Again, the subscript ‘s’ refers to the modified surface. In our case, ‘s’ refers to the roof but
 149 the definition of ACE_s is more general and not specific to the roof surface. Here it should

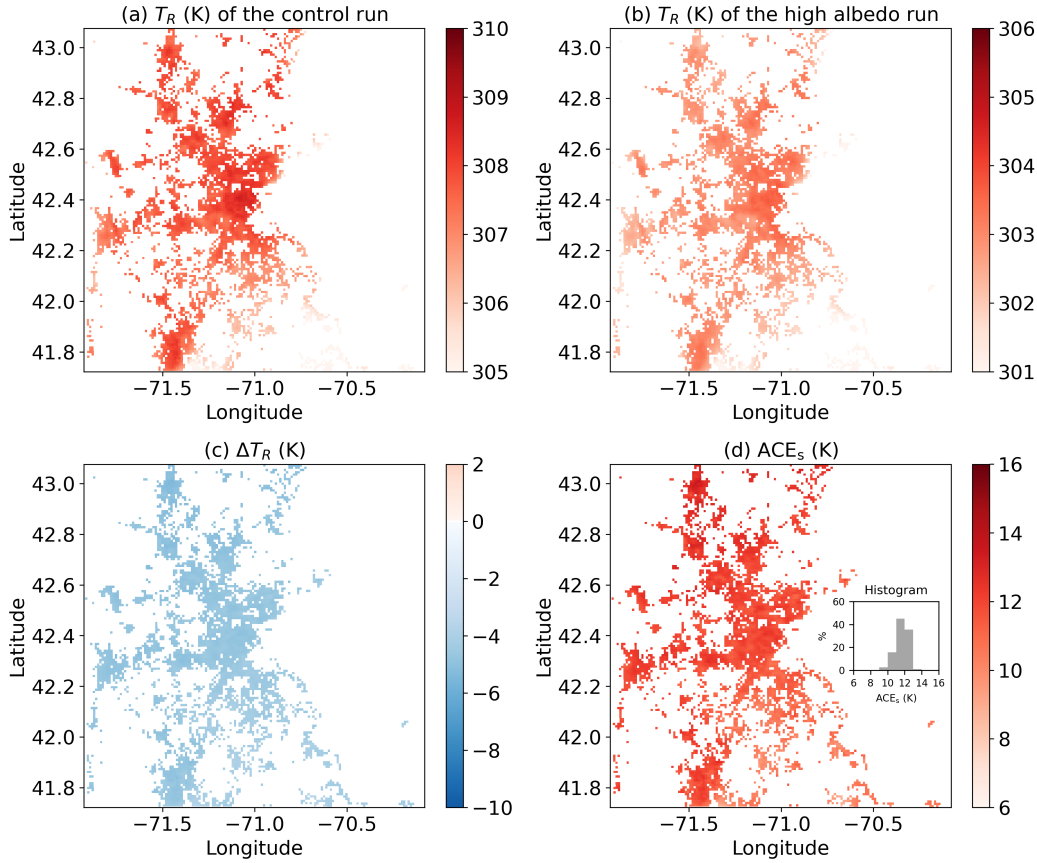


Figure 4: Similar to Figure 2 but for roof surface temperature (T_R). (a) T_R of the control run (K), (b) T_R of the high albedo run (K), (c) ΔT_R (K), (d) ACE_s (K). The inset in (d) shows the histogram of ACE_s . Only the results over urban grid cells are shown and the results are averaged over a 5-day period from July 20 to July 24, 2022.

150 also be pointed out that throughout the paper T_s , even when defined generally, refers to the
 151 surface temperature of a facet (e.g., roof, wall, canyon floor, etc) shown in Figure 1. This is
 152 different from $T_{surface}$ in Figure 1(b, d), which refers to an aggregated surface temperature
 153 of the entire grid cell. In WRF, $T_{surface}$ is not simply an area-weighted average of the surface
 154 temperatures across all urban facets; instead, its calculation is based on an energy balance
 155 approach and hence $\Delta T_{surface} \neq \Delta T_{sf}$ [10, 12].

156 3 Albedo Cooling Sensitivity (ACS)

157 3.1 From Cooling Effectiveness to Climate Sensitivity

158 In climate science, changes in global average temperature (ΔT , K) are often interpreted with
 159 the associated climate forcing (ΔF , $W m^{-2}$), which is quantified at the top of the atmosphere
 160 and is commonly referred to as the radiative forcing. While quantifying climate forcing at the
 161 top of the atmosphere for the white roof problem may be challenging (and unnecessary if we
 162 focus on local temperature changes), we can apply a similar concept at the surface. From the
 163 surface perspective, the forcing in the white roof problem can be expressed as $SW_{in}(-\Delta\alpha)$,
 164 namely, the change of absorbed shortwave radiation assuming that SW_{in} remains constant
 165 when the surface albedo is altered. Hence, instead of linking ΔT to $\Delta\alpha$ as in the ACE

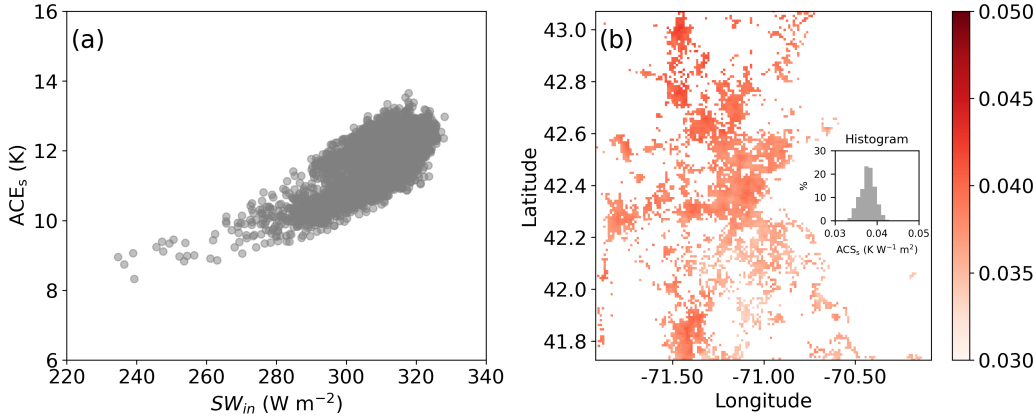


Figure 5: (a) The relation between ACE_s (K) and incoming shortwave radiation (SW_{in} , $W m^{-2}$). (b) The spatial pattern of ACS_s ($K W^{-1} m^2$). The inset in (b) shows the histogram of ACS_s . Only the results over urban grid cells are shown and the results are averaged over a 5-day period from July 20 to July 24, 2022.

166 framework, a climate science inspired approach would be linking ΔT to $SW_{in}(-\Delta\alpha)$.

167 To differentiate from ACE, this new index will be referred to as the Albedo Cooling
 168 Sensitivity (ACS). Given that the forcing used is a surface forcing, ACS probably will work
 169 better for understanding surface temperature changes. To emphasize this focus on surface
 170 temperature, a subscript ‘s’ is added to ΔT , $\Delta\alpha$ and ACS, as follows:

$$171 \quad ACS_s = \frac{\Delta T_s}{SW_{in}(-\Delta\alpha_s)} = -\frac{\Delta T_s}{SW_{in}\Delta\alpha_s} = \frac{ACE_s}{SW_{in}}. \quad (3)$$

172 The ACS_s defined this way has a standard unit of $K W^{-1} m^2$ and can be interpreted as a local
 173 surface climate sensitivity. Comparing Eq. 3 to Eq. 1, it is clear that ACS_s specifically focuses
 174 on surface temperature while ACE focuses on near-surface air temperature. Comparing Eq.
 175 3 to Eq. 2 reveals that ACS_s addresses the SW_{in} dependence of ACE_s , as shown in Figure 5a.
 176 Not surprisingly, the stronger the SW_{in} , the larger the ACE_s . However, the scatter in Figure
 177 5a suggests that ACS_s is not a constant, whose spatial pattern is shown in Figure 5b. To
 178 understand the spatial variability of ACS_s , a linearized surface energy balance (SEB) model
 179 [1, 13] is utilized, as discussed below.

180 3.2 A Linearized Surface Energy Balance (SEB) Model for ACS_s

181 For a homogeneous surface (e.g., the roof surface in the SLUCM model), the SEB equation
 182 can be written as:

$$183 \quad SW_{in}(1 - \alpha_s) + \varepsilon LW_{in} = H + LE + G + \varepsilon\sigma T_s^4 \quad (4)$$

184 where SW_{in} and LW_{in} are the incoming shortwave and longwave radiation ($W m^{-2}$), re-
 185 spectively, ε is the surface emissivity, H is the sensible heat flux ($W m^{-2}$), LE is the latent
 186 heat flux ($W m^{-2}$), G is the conductive or ground heat flux ($W m^{-2}$), and $\varepsilon\sigma T_s^4$ is the emit-
 187 ted longwave radiation by the surface ($W m^{-2}$) where σ is the Stefan-Boltzmann constant
 188 ($=5.67 \times 10^{-8} W m^{-2} K^{-4}$) and T_s is the temperature of the surface (K) to which this SEB
 189 equation applies. The emitted longwave radiation is rearranged to the right-hand-side of the
 190 surface energy balance equation to emphasize that each term on the right-hand-side of Eq. 4 is
 191 a function of T_s while the terms on the left-hand-side of Eq. 4 are assumed to be atmospheric
 192 forcing for the surface and are not directly affected by T_s .

193 Each term on the right-hand-side of Eq. 4 is then linearized:

194
$$H = \lambda_H T_s + C_H, \quad (5)$$

195
$$LE = \lambda_{LE} T_s + C_{LE} \quad (6)$$

196
$$G = \lambda_G T_s + C_G, \quad (7)$$

197
$$\varepsilon \sigma T_s^4 = \lambda_{ELW} T_s + C_{ELW}. \quad (8)$$

201 Here λ s and C s are the slopes and intercepts of these linear relations, respectively. The
 202 λ s can be viewed as heat transfer efficiencies which have standard units of $\text{W m}^{-2} \text{K}^{-1}$.
 203 The C s have standard units of W m^{-2} . The full expressions of λ s and C s can be found
 204 elsewhere [1, 13] and thus only the key controls of λ s and C s are briefly mentioned here.
 205 The convective heat transfer efficiency λ_H depends primarily on the wind speed and thermal
 206 stratification; the latent heat transfer efficiency λ_{LE} also depends on the wind speed and
 207 thermal stratification, but more importantly on the moisture and vegetation characteristics of
 208 the surface; the conductive heat transfer efficiency λ_G is mostly controlled by the heat capacity
 209 and thermal conductivity of the ground (or the roof material in our case); the longwave
 210 radiative heat transfer efficiency λ_{ELW} is only a function of the current air temperature. For
 211 the intercepts, C_H depends on the air temperature. Note that in the WRF-SLUCM model,
 212 the roof directly interacts with the atmosphere above the canyon. In other words, H is
 213 formulated based on the difference between the roof surface temperature and the atmospheric
 214 temperature above the canyon (T_A , see Figure 1). As a result, C_H depends on T_A in WRF-
 215 SLUCM. The intercept C_{LE} depends on the air temperature and air humidity; C_G depends
 216 on the deep ground temperature (for the roof in WRF-SLUCM, C_G depends on the building
 217 interior temperature); C_{ELW} is only a function of the current air temperature. For completely
 218 dry and non-evaporating roofs, $\lambda_{LE} = 0$ and $C_{LE} = 0$.

219 With this linear assumption, the SEB can be interpreted using Figure 6, where the hor-
 220 izontal black solid line represents the left-hand-side of Eq. 4 and is independent of T_s while
 221 the red line represents the right-hand-side Eq. 4 and is a linear function of T_s with a slope
 222 of $\lambda_H + \lambda_{LE} + \lambda_G + \lambda_{ELW}$. The intersection of these two lines indicates an energy balance
 223 state. When the surface albedo is increased by $\Delta\alpha_s$, the left-hand-side of Eq. 4 is reduced
 224 by $SW_{in}(-\Delta\alpha_s)$, assuming that SW_{in} and εLW_{in} remain constant. On Figure 6, it means
 225 that the horizontal black solid line is moved downward by $SW_{in}(-\Delta\alpha_s)$ (i.e., it becomes the
 226 horizontal black dashed line). Further assuming that the red line stays where it is, the change
 227 in the surface temperature can be readily obtained from simple geometry on Figure 6, as
 228 follows:

229
$$\Delta T_s = \frac{SW_{in}(-\Delta\alpha_s)}{\lambda_H + \lambda_{LE} + \lambda_G + \lambda_{ELW}}, \quad (9)$$

230 which gives

231
$$ACS_s = \frac{\Delta T_s}{SW_{in}(-\Delta\alpha_s)} = \frac{1}{\lambda_H + \lambda_{LE} + \lambda_G + \lambda_{ELW}}. \quad (10)$$

232 The beauty of ACS_s , as now demonstrated in Eq. 10, is that it can be related to various
 233 heat transfer efficiencies. These heat transfer efficiencies are equivalent to climate feedback
 234 parameters widely used in the climate science literature. Therefore, one might argue that by
 235 introducing the ACS_s index and utilizing the linearized SEB model, the white roof problem,
 236 which has long been approached from the perspective of applied meteorology, is now reframed
 237 as a climate science problem. Eq. 10 clearly shows that ACS_s cannot be a constant as the
 238 heat transfer efficiencies or climate feedback parameters vary with meteorological and surface
 239 conditions [1, 13].

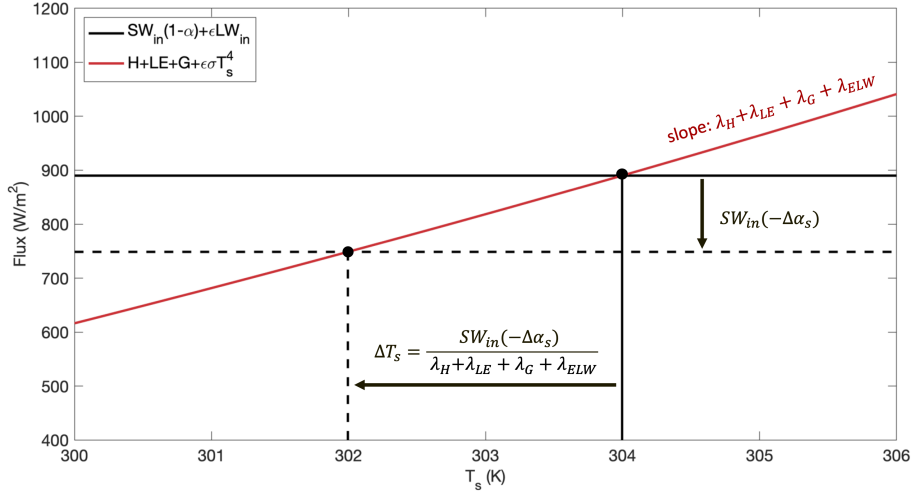


Figure 6: A linearized SEB model for ACS_s . The black solid line (horizontal) represents the left-hand-side of Eq. 4 and is independent of T_s while the red line represents the right-hand-side Eq. 4 and is a linear function of T_s with a slope of $\lambda_H + \lambda_{LE} + \lambda_G + \lambda_{ELW}$. The intersection of these two lines indicates an energy balance state. The black dashed line (horizontal) represents the left-hand-side of Eq. 4 when the albedo is increased by $\Delta\alpha_s$.

Eq. 10 is the simplest case where the four feedbacks are the most fundamental, stabilizing feedbacks in the studied system (in this case, the surface). By analogy, they are similar to the Planck feedback (also referred to as the Planck response) in the context of global climate change. One can incorporate additional feedback parameters. To do so, the right-hand-side of the SEB equation (Eq. 4) is first denoted as R , namely, $R = H + LE + G + \varepsilon\sigma T_s^4$. The difference caused by an increase in the roof albedo on both sides of the SEB equation still has to be balanced, namely, $\Delta [SW_{in}(1 - \alpha_s) + \varepsilon LW_{in}] = \Delta R$. Further assuming that SW_{in} and εLW_{in} are not affected by the increase in roof albedo results in $SW_{in}(-\Delta\alpha_s) = \Delta R$. Hence, the ACS_s can be expressed as

$$ACS_s = \frac{\Delta T_s}{SW_{in}(-\Delta\alpha_s)} = \frac{\Delta T_s}{\Delta R} = \frac{1}{\frac{\Delta R}{\Delta T_s}}. \quad (11)$$

Since $R = H + LE + G + \varepsilon\sigma T_s^4 = (\lambda_H + \lambda_{LE} + \lambda_G + \lambda_{ELW})T_s + (C_H + C_{LE} + C_G + C_{ELW})$, we can further derive

$$\begin{aligned} \frac{\Delta R}{\Delta T_s} &= \frac{\partial R}{\partial T_s} \\ &+ \frac{\partial R}{\partial \lambda_H} \frac{\Delta \lambda_H}{\Delta T_s} + \frac{\partial R}{\partial \lambda_{LE}} \frac{\Delta \lambda_{LE}}{\Delta T_s} + \frac{\partial R}{\partial \lambda_G} \frac{\Delta \lambda_G}{\Delta T_s} + \frac{\partial R}{\partial \lambda_{ELW}} \frac{\Delta \lambda_{ELW}}{\Delta T_s} \\ &+ \frac{\partial R}{\partial C_H} \frac{\Delta C_H}{\Delta T_s} + \frac{\partial R}{\partial C_{LE}} \frac{\Delta C_{LE}}{\Delta T_s} + \frac{\partial R}{\partial C_G} \frac{\Delta C_G}{\Delta T_s} + \frac{\partial R}{\partial C_{ELW}} \frac{\Delta C_{ELW}}{\Delta T_s}, \end{aligned} \quad (12)$$

where

$$\frac{\partial R}{\partial T_s} = \lambda_H + \lambda_{LE} + \lambda_G + \lambda_{ELW}. \quad (13)$$

Substituting Eqs. 12 and 13 into Eq. 11 yields a full equation for ACS_s , as follows:

$$ACS_s = \frac{1}{\lambda_H + \lambda_{LE} + \lambda_G + \lambda_{ELW} + \frac{\partial R}{\partial \lambda_H} \frac{\Delta \lambda_H}{\Delta T_s} + \frac{\partial R}{\partial \lambda_{LE}} \frac{\Delta \lambda_{LE}}{\Delta T_s} + \frac{\partial R}{\partial \lambda_G} \frac{\Delta \lambda_G}{\Delta T_s} + \frac{\partial R}{\partial \lambda_{ELW}} \frac{\Delta \lambda_{ELW}}{\Delta T_s} + \frac{\partial R}{\partial C_H} \frac{\Delta C_H}{\Delta T_s} + \frac{\partial R}{\partial C_{LE}} \frac{\Delta C_{LE}}{\Delta T_s} + \frac{\partial R}{\partial C_G} \frac{\Delta C_G}{\Delta T_s} + \frac{\partial R}{\partial C_{ELW}} \frac{\Delta C_{ELW}}{\Delta T_s}}. \quad (14)$$

258 It is now clear that Eq. 10 is a simplified version of Eq. 14 by assuming $\Delta R/\Delta T_s \approx \partial R/\partial T_s$
 259 (or equivalently, by assuming the red line on Figure 6 remains unchanged when the surface
 260 albedo is altered). This assumption is not always valid. For example, λ_H might change when
 261 the surface albedo is altered, as atmospheric stability increases and convective heat transfer
 262 becomes less efficient with a higher surface albedo due to reduced sensible heat flux. This
 263 change of λ_H alters the slope of the red line on Figure 6. The significance of such feedback
 264 can be quantified by the term $\frac{\partial R}{\partial \lambda_H} \frac{\Delta \lambda_H}{\Delta T_s}$, which can be viewed as a new feedback parameter.
 265 However, fully understanding the importance of these new feedback parameters is outside the
 266 scope of this study.

267 Before applying Eq. 10 to analyzing the WRF simulation results, it is important to
 268 comment on the relevant time scales. Eq. 10 relies on the linear relations between four
 269 fluxes and surface temperature (Eqs. 5-8) and ignores many feedbacks such as the change of
 270 λ_H . These assumptions tend to work better at long-term time scales (e.g., averages over all
 271 summer months within a 30-year period). At long-term time scales, Eq. 10 can be used to
 272 interpret the spatial variability [22] and other variability (e.g., introduced by varying model
 273 parameterizations) of white roof effects. At short time scales, Eq. 10 has to be used carefully
 274 or should not be used. For example, Eq. 10 cannot be used to interpret the nighttime
 275 effects of white roofs, since treating $SW_{in}(-\Delta\alpha)$ as the forcing is problematic at night when
 276 the incoming shortwave radiation is zero. This is partly why the WRF results presented
 277 earlier have been averaged over the entire simulation period, without separating daytime
 278 from nighttime. However, the time scale remains short since the WRF simulations only span
 279 five days. Whether Eq. 10 can be used to interpret the spatial variability of white roof effects
 280 at multi-day time scales remains unclear, which frames the scope of the following section.
 281 Here it's noted that multi-day simulations are commonly used to assess white roof effects in
 282 the urban climate literature [e.g. 11, 14, 18, 26] and thus addressing the applicability of Eq.
 283 10 at multi-day time scales has practical value.

284 3.3 The Variability of ACS_s and the Role of Convective Heat Transfer Ef- 285 ficiency

286 As alluded to earlier, in this section Eq. 10 is used to interpret the spatial variability of
 287 ACS_s simulated by WRF, as shown in Figure 5b. This spatial variability represents the
 288 neighborhood-to-neighborhood variability, not the city-to-city variability. Moreover, two sen-
 289 sitivity cases are conducted where different planetary boundary layer (including surface layer)
 290 parameterizations are used. The planetary boundary layer (including surface layer) param-
 291 eterizations represent the effects of turbulence and turbulent transport in the atmosphere,
 292 which can strongly modulate the dynamics of surface temperature and near-surface air tem-
 293 perature. Specifically, the default case (results already presented earlier) uses the YSU scheme
 294 [4, 5], and the two sensitivity cases use the MYNN [15, 16] and MYJ [6, 15] schemes, respec-
 295 tively. These sensitivity tests are not meant to be exhaustive, but rather to demonstrate the
 296 utility of Eq. 10.

297 Figure 7(a, b, c) show the probability density functions (PDFs) of ACE (defined again
 298 based on T_2), ACE_s, and ACS_s, respectively. The PDFs are estimated using Kernel density
 299 estimation, a non-parametric method that smooths discrete data points into a continuous
 300 distribution. It is clear that all three indices vary spatially within each case and vary across
 301 cases. The ACE values range from -5 to 10 K, the ACE_s values vary between 8 and 14 K,
 302 while the ACS_s values range between 0.03 and 0.045 K W⁻¹ m². Interestingly, when the YSU
 303 scheme is replaced by the MYNN and MYJ schemes, the negative ACE values become much
 304 less. These results indicate that the simulated white roof effects are sensitive to turbulence
 305 parameterizations.

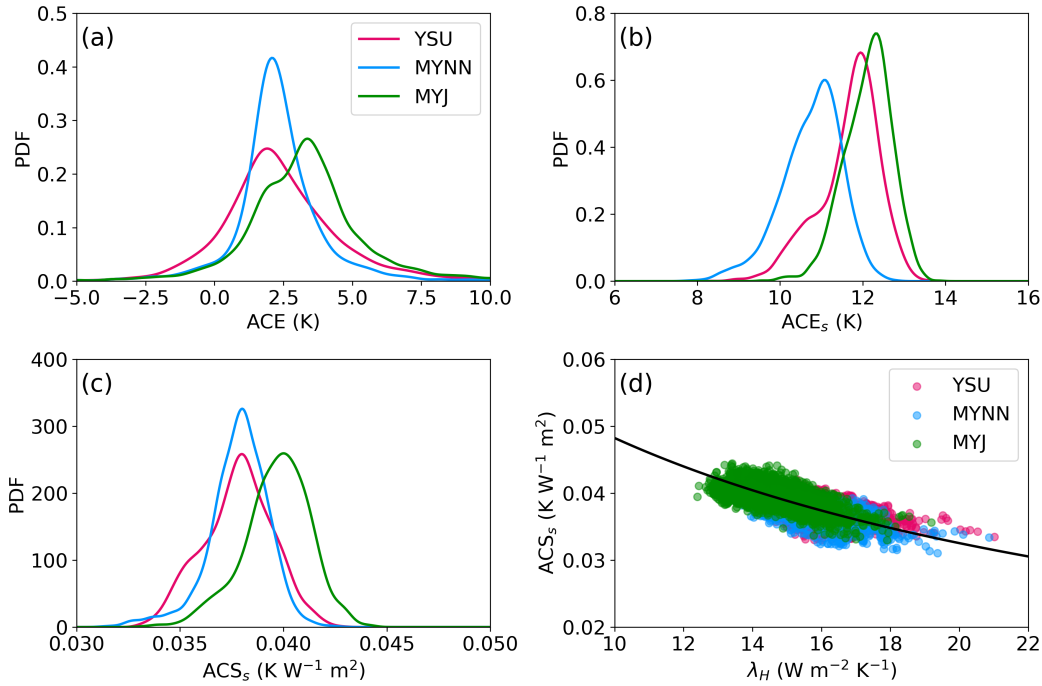


Figure 7: PDFs of (a) ACE, (b) ACE_s , (c) ACS_s ; (d) the relation between ACS_s and λ_H where the black line is a fitted curve based on Eq. 10, given by $ACS_s = 1/(\lambda_H + 10.73)$. Only the results over urban grid cells are included and the results are averaged over a 5-day period from July 20 to July 24, 2022.

306 While the values of ACS_s cannot be directly compared to those of ACE_s and ACE due to differences in their dimensions, we can use the coefficients of variation, which are dimensionless, to characterize their variability. For each case where the variability is due to spatial variations, the coefficients of variation for ACS_s and ACE_s are of the same order of magnitude, but are an order of magnitude smaller than those for ACE. Comparing ACS_s to ACE_s , the coefficients of variation are always smaller for ACS_s ; namely, the variability of ACS_s is more constrained than that of ACE_s . This result implies that part of the spatial variability associated with ACE_s is caused by the spatial variability of SW_{in} , as can be inferred from Figure 5a.

315 When compared across different cases, the MYNN case has very different ACE_s values compared to the YSU case, but their ACS_s values are similar. This is due to the fact that SW_{in} are different between these two cases (Figure 8a). Therefore, normalizing $-\Delta T_s/\Delta\alpha_s$ by SW_{in} (i.e., moving from ACE_s to ACS_s) helps reduce the variability caused by SW_{in} across cases. Note that the variability of SW_{in} caused by changing turbulence parameterizations is quite small (on the order of 20-40 $W m^{-2}$, as can be seen from Figure 8a). Even for such small variability of SW_{in} , it is still better to approach the roof surface temperature change from the perspective of ACS_s rather than ACE_s . For large variability of SW_{in} (e.g., when studying city-to-city variability or seasonal variability of white roof effects), normalizing $-\Delta T_s/\Delta\alpha_s$ by SW_{in} will be more important as shall be seen later.

325 MYJ and YSU cases have similar SW_{in} (Figure 8a), yet their ACS_s values differ strongly (Figure 7c), suggesting that other factors must influence the results. Close inspection reveals that the MYJ case has a smaller near-surface wind speed than the YSU case (Figure 8b). The linearized SEB model provides the necessary tools to understand why ACS_s is increased with reduced near-surface wind speed. As shown in Figure 7d, ACS_s is a strong function of

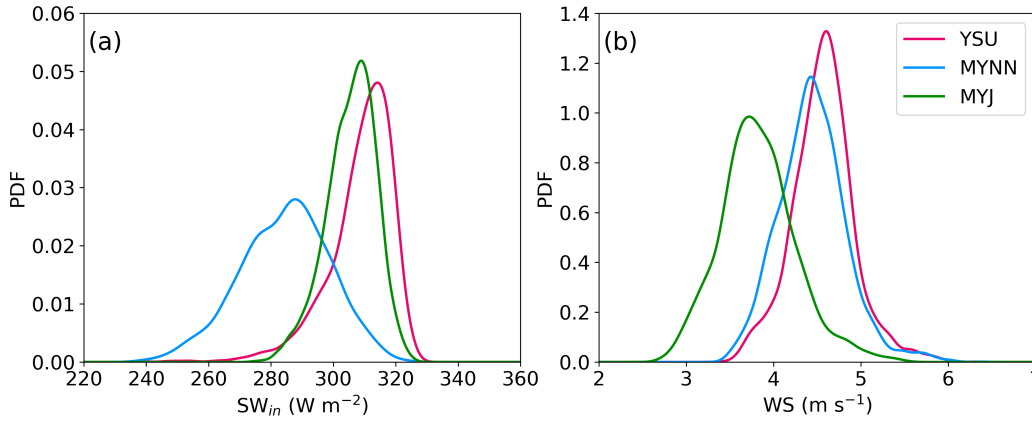


Figure 8: PDFs of (a) SW_{in} and (b) 10-m wind speed (WS) in the control runs (i.e., the roof albedo of 0.2). Only the results over urban grid cells are included and the results are averaged over a 5-day period from July 20 to July 24, 2022.

330 λ_H , the convective heat transfer efficiency. In neighborhoods with weaker convective heat
 331 transfer efficiency caused by reduced near-surface wind speed, the ACS_s values are larger
 332 (c.f. MYJ to YSU in Figure 7c, d). Physically, this occurs because with weaker convective
 333 heat transfer efficiency, the roof surface temperature tends to be much higher, as less heat is
 334 transferred into the atmosphere. Under such conditions, increasing the roof albedo results in
 335 a more pronounced reduction in roof surface temperature. Conversely, when heat is efficiently
 336 convected into the atmosphere and the roof surface temperature is already low, increasing the
 337 roof albedo has a smaller impact.

338 However, the objective here is not to determine why different planetary boundary layer
 339 parameterizations yield varying SW_{in} and wind speed. Instead, the focus is on interpreting the
 340 simulated ACS_s using the linearized SEB model (Eq. 10). For each case, the spatial variability
 341 of λ_H is found to be a key control of the spatial variability of ACS_s , as shown in Figure 7d. To
 342 fully grasp this point, we need to take a closer look at the four climate feedback parameters in
 343 these WRF simulations. As discussed, λ_H is the convective heat transfer efficiency and thus
 344 depends on the wind speed and thermal stratification. Hence, λ_H is expected to vary spatially
 345 (and with turbulence parameterizations). In these simulations, λ_H varies between 12 to 22
 346 $W m^{-2} K^{-1}$, as shown in Figure 7d. On the other hand, λ_{LE} , λ_G , and λ_{ELW} have limited
 347 spatial variability in these simulations. During the simulation period, there is no rainfall and
 348 the roof is completely dry, leading to $\lambda_{LE} = 0$. The λ_G is largely determined by roof thermal
 349 properties (especially heat capacity and thermal conductivity)[13], which are prescribed inputs
 350 and do not vary across the domain [12]. The λ_{ELW} scales with T_A^3 and thus does not vary
 351 strongly in space given that T_A is generally on the order of 300 K, yielding $\lambda_{ELW} \approx 6 W m^{-2}$
 352 K^{-1} . The function $ACS_s = 1/(\lambda_H + C)$ (the black line in Figure 7d) provides a good fit to
 353 the simulation results, where C is determined via nonlinear least squares regression as 10.73
 354 ± 0.02 . The fitted C value (unit: $W m^{-2} K^{-1}$) and that $\lambda_{ELW} \approx 6 W m^{-2} K^{-1}$ suggest
 355 that $\lambda_G \approx 4.7 W m^{-2} K^{-1}$. This is consistent with previous work suggesting that λ_G has
 356 similar magnitude as λ_{ELW} but is much smaller than λ_H [1]. In summary, only λ_H exhibits
 357 strong spatial variability in these simulations, while the spatial variability of the other three
 358 feedback parameters is limited, explaining why the spatial variability of λ_H is a key control of
 359 the spatial variability of ACS_s . This does not mean that the spatial variability of these other
 360 feedback parameters is always not important. Since they are dependent on meteorological
 361 conditions and urban hygrothermal properties, their spatial variability may become relevant

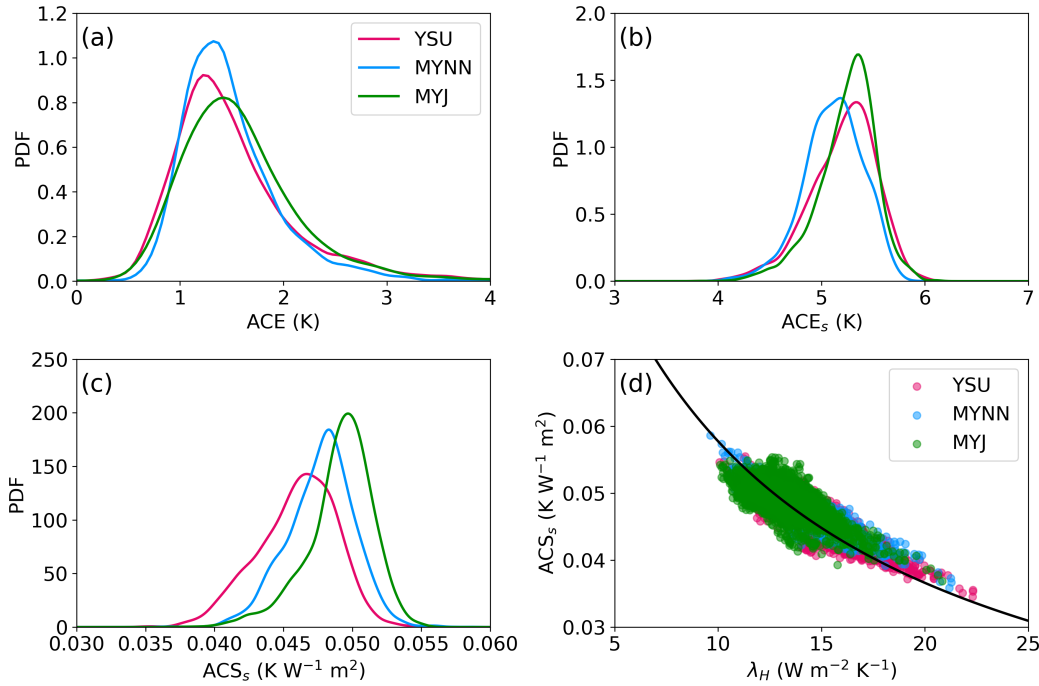


Figure 9: PDFs of (a) ACE, (b) ACE_s , (c) ACS_s ; (d) the relation between ACS_s and λ_H where the black line is a fitted curve based on Eq. 10, given by $ACS_s = 1/(\lambda_H + 7.31)$. Only the results over urban grid cells are included and the results are averaged over a 5-day period from Feb 10 to Feb 14, 2022.

362 under certain circumstances [22].

363 To corroborate these findings, similar simulations are conducted for a wintertime period
 364 (Feb 10-14, 2022, with a spin-up day of Feb 9) when the average incoming solar radiation is
 365 about 100 W m^{-2} (i.e., about 1/3 of the average incoming solar radiation during the summer-
 366 time period). The analysis is repeated and results are shown in Figure 9. Comparing Figure 9
 367 to Figure 7 reveals that the ACE and ACE_s values differ strongly between summer and winter
 368 periods. In contrast, the ACS_s values are more consistent between the two periods. Among
 369 the three indices, the coefficients of variation are the smallest for ACS_s , again highlighting the
 370 importance of normalization by SW_{in} . Moreover, the variability of ACS_s is largely explained
 371 by λ_H (e.g., the MYJ case again has the largest ACS_s values because of the smallest near-
 372 surface wind speeds). However, the fitted line in Figure 9d becomes $ACS_s = 1/(\lambda_H + 7.31)$.
 373 The value of 7.31 ± 0.01 (unit: $\text{W m}^{-2} \text{ K}^{-1}$) is reduced compared to its summer counterpart,
 374 partly due to the reduction of λ_{ELW} to about $4.5 \text{ W m}^{-2} \text{ K}^{-1}$ at 270 K.

375 These results demonstrate the utility of the linearized SEB framework. While not all
 376 feedback parameters are readily available or can be easily computed such as λ_G at short time
 377 scales, the physical insights offered by the linearized SEB framework underscore its value as
 378 a *diagnostic* tool for understanding the variability of ACS_s .

379 4 Final Remarks

380 By focusing on the roof surface temperature and utilizing concepts like climate forcing, sen-
 381 sitivity, and feedback, the white roof problem is reframed as a climate science problem. A
 382 new index called Albedo Cooling Sensitivity (ACS_s) is proposed and a linearized SEB model
 383 is utilized to understand the variability of ACS_s . The spatial variability of ACS_s simulated

384 by WRF and the influence of turbulence parameterizations on ACS_s are examined, where the
385 convective heat transfer efficiency is found to play an important role.

386 The purpose of this paper is not to discredit the concept of ACE, but rather to provide
387 a stepping stone towards understanding the white roof effects. The ACS_s concept could
388 and perhaps should be used jointly with ACE. More broadly, approaching urban adaptation
389 challenges from the perspective of climate science can generate new insights that could not
390 be obtained if these problems were only treated in the realm of applied meteorology. The use
391 of concepts of forcing, sensitivity, and feedback should be embraced. A few more research
392 examples are briefly discussed to emphasize the value of these concepts. First, [23] examined
393 the cooling benefits of irrigation on green roofs and treated the change of latent heat flux due
394 to irrigation as the forcing (unlike in the model presented here where the change of latent
395 heat flux is viewed as a response). Their model successfully explained the spatial variability
396 of cooling benefits of green roof irrigation. Second, previous studies found that urban trees'
397 cooling efficiency, defined as the magnitude of land surface temperature reduction per 1%
398 increase in fractional tree cover, tends to be stronger in hot and dry cities [25]. This can be
399 understood again from the perspective of changes in the latent heat flux (the forcing): a 1%
400 increase in fractional tree cover tends to result in a stronger increase in latent heat flux in
401 hot and dry regions than in cool and humid regions where latent heat flux is more controlled
402 by energy availability. Third, [24] reviewed previous modeling studies on the warming effects
403 of anthropogenic heat flux (Q_{AH}) and found large discrepancies in terms of changes of urban
404 air temperature (ΔT) due to anthropogenic heat fluxes. However, the sensitivity of urban air
405 temperature to anthropogenic heat flux ($\Delta T/\Delta Q_{AH}$) showed consistency across studies. They
406 further found that feedbacks introduced by convective heat transfer efficiency and its variation
407 were key to explaining the seasonal variations of $\Delta T/\Delta Q_{AH}$. These research examples further
408 demonstrate the power of concepts of climate forcing, sensitivity, and feedback in urban
409 adaptation research.

410 Lastly, can concepts of climate forcing, sensitivity, and feedback still offer insights if the
411 focus was near-surface air temperature? This remains an open question. First, even for the
412 white roof problem it is unclear whether $SW_{in}(-\Delta\alpha)$ represents a forcing for the near-surface
413 air, as it does not enter the energy budget of near-surface air. Perhaps a better candidate is
414 ΔH , which is still related to $SW_{in}(-\Delta\alpha)$ especially at long-term time scales. Second, unlike
415 the one-dimensional SEB equation which provides a framework for understanding surface
416 temperature dynamics, the energy budget of near-surface air is three-dimensional (unless
417 some idealization is applied to the near-surface air such as the urban canopy air in SLUCMs
418 [24] or the constant flux layer [21]) and thus much more complicated. It is unclear whether
419 the near-surface air budget can provide the same general framework like the SEB equation
420 based on which sensitivities and feedback parameters can be connected. Addressing these
421 challenges are left for future work.

422 Acknowledgements

423 This research was supported by the U.S. Department of Energy, Office of Science, as part of
424 research in MultiSector Dynamics, Earth and Environmental System Modeling Program. The
425 work used resources of the National Energy Research Scientific Computing Center (NERSC),
426 a U.S. Department of Energy Office of Science User Facility located at Lawrence Berkeley
427 National Laboratory, operated under Contract No. DE-AC02-05CH11231, as well as the high-
428 performance computing support from Derecho (<https://doi.org/10.5065/qx9a-pg09>) provided
429 by NCAR's Computational and Information Systems Laboratory, sponsored by the National
430 Science Foundation. This research was also supported by an unrestricted gift from Google,
431 but the statements, findings, and conclusions do not necessarily reflect the views of Google.

432 Finally, I would like to thank Mingze Ding, Xiaojing Tang, and Ting Sun for reviewing earlier
433 versions of this essay, and Lucy Hutyra, David Fork, Jiachuan Yang, and Ning Zhang for
434 valuable discussions. The comments from two anonymous reviewers are also acknowledged.

435 Data Availability

436 The WRF outputs of this work were produced with a modified version of WRF v4.2.2, which
437 can be found at <https://doi.org/10.5281/zenodo.14611848>. The scripts to reproduce the fig-
438 ures are documented at https://github.com/IMMM-SFA/li_2025_ARC/tree/main.

439 Author Contributions

440 **DL:** Conceptualization; Data Curation; Formal Analysis; Funding Acquisition; Methodology;
441 Software; Visualization; Writing – Original Draft Preparation; Writing – Review & Editing.

442 References

- 443 [1] S. Bateni and D. Entekhabi. Relative efficiency of land surface energy balance compo-
444 nents. *Water Resources Research*, 48(4), 2012.
- 445 [2] S. A. Changnon. Applied climatology: The golden age has begun. *Bulletin of the Ameri-
446 can Meteorological Society*, 86(7):915–919, 2005.
- 447 [3] J. Garratt, J. Wilczak, A. Holtslag, H. P. Schmid, A. Grachev, A. Beljaars, T. Foken,
448 F. Chen, C. Fairall, B. Hicks, et al. Commentaries on top-cited boundary-layer meteo-
449 rology articles. *Boundary-Layer Meteorology*, 177:169–188, 2020.
- 450 [4] S.-Y. Hong. A new stable boundary-layer mixing scheme and its impact on the simulated
451 East Asian summer monsoon. *Quarterly Journal of the Royal Meteorological Society*, 136
452 (651):1481–1496, 2010.
- 453 [5] S.-Y. Hong, Y. Noh, and J. Dudhia. A new vertical diffusion package with an explicit
454 treatment of entrainment processes. *Monthly weather review*, 134(9):2318–2341, 2006.
- 455 [6] Z. Janjic. Nonsingular implementation of the Mellor-Yamada Level 2.5 Scheme in the
456 NCEP Meso model, National Centers for Environmental Prediction. *Office Note# 437*,
457 pages 1–61, 2001.
- 458 [7] E. S. Krayenhoff and J. A. Voogt. Impacts of urban albedo increase on local air temper-
459 ature at daily–annual time scales: Model results and synthesis of previous work. *Journal
460 of Applied Meteorology and Climatology*, 49(8):1634–1648, 2010.
- 461 [8] E. S. Krayenhoff, A. M. Broadbent, L. Zhao, M. Georgescu, A. Middel, J. A. Voogt,
462 A. Martilli, D. J. Sailor, and E. Erell. Cooling hot cities: a systematic and critical review
463 of the numerical modelling literature. *Environmental Research Letters*, 16(5):053007,
464 2021.
- 465 [9] H. Kusaka, H. Kondo, Y. Kikegawa, and F. Kimura. A simple single-layer urban canopy
466 model for atmospheric models: Comparison with multi-layer and slab models. *Boundary-
467 layer meteorology*, 101:329–358, 2001.
- 468 [10] D. Li and E. Bou-Zeid. Quality and sensitivity of high-resolution numerical simulation
469 of urban heat islands. *Environmental Research Letters*, 9(5):055001, 2014.

- 470 [11] D. Li, E. Bou-Zeid, and M. Oppenheimer. The effectiveness of cool and green roofs as
471 urban heat island mitigation strategies. *Environmental Research Letters*, 9(5):055002,
472 2014.
- 473 [12] D. Li, T. Sun, J. Yang, N. Zhang, P. Vahmani, and A. Jones. Structural uncertainty in
474 the sensitivity of urban temperatures to anthropogenic heat flux. *Journal of Advances
475 in Modeling Earth Systems*, 16(10):e2024MS004431, 2024.
- 476 [13] D. Li, L. Wang, W. Liao, T. Sun, G. Katul, E. Bou-Zeid, and B. Maronga. Persistent
477 urban heat. *Science Advances*, 10(15):eadj7398, 2024.
- 478 [14] X.-X. Li and L. K. Norford. Evaluation of cool roof and vegetations in mitigating urban
479 heat island in a tropical city, Singapore. *Urban Climate*, 16:59–74, 2016.
- 480 [15] G. L. Mellor and T. Yamada. Development of a turbulence closure model for geophysical
481 fluid problems. *Reviews of Geophysics*, 20(4):851–875, 1982.
- 482 [16] M. Nakanishi and H. Niino. Development of an improved turbulence closure model for
483 the atmospheric boundary layer. *Journal of the Meteorological Society of Japan. Ser. II*,
484 87(5):895–912, 2009.
- 485 [17] Y. Qin, W. Liao, and D. Li. Attributing the urban–rural contrast of heat stress simulated
486 by a global model. *Journal of Climate*, 36(6):1805–1822, 2023.
- 487 [18] A. Sharma, P. Conry, H. Fernando, A. F. Hamlet, J. Hellmann, and F. Chen. Green
488 and cool roofs to mitigate urban heat island effects in the Chicago metropolitan area:
489 Evaluation with a regional climate model. *Environmental Research Letters*, 11(6):064004,
490 2016.
- 491 [19] W. C. Skamarock, J. B. Klemp, J. Dudhia, D. O. Gill, Z. Liu, J. Berner, W. Wang,
492 J. Powers, M. Duda, D. Barker, et al. A description of the advanced research WRF
493 version 4. *NCAR tech. note ncar/tn-556+ str*, 145, 2019.
- 494 [20] C. Souch and S. Grimmond. Applied climatology: urban climate. *Progress in physical
495 geography*, 30(2):270–279, 2006.
- 496 [21] L. Wang and D. Li. Urban heat islands during heat waves: A comparative study between
497 Boston and Phoenix. *Journal of Applied Meteorology and Climatology*, 60(5):621–641,
498 2021.
- 499 [22] L. Wang, M. Huang, and D. Li. Where are white roofs more effective in cooling the
500 surface? *Geophysical Research Letters*, 47(15):e2020GL087853, 2020.
- 501 [23] L. Wang, M. Huang, and D. Li. Strong influence of convective heat transfer efficiency
502 on the cooling benefits of green roof irrigation. *Environmental Research Letters*, 16(8):
503 084062, 2021.
- 504 [24] L. Wang, T. Sun, W. Zhou, M. Liu, and D. Li. Deciphering the sensitivity of urban
505 canopy air temperature to anthropogenic heat flux with a forcing-feedback framework.
506 *Environmental Research Letters*, 18(9):094005, 2023.
- 507 [25] Q. Yang, X. Huang, X. Tong, C. Xiao, J. Yang, Y. Liu, and Y. Cao. Global assessment
508 of urban trees’ cooling efficiency based on satellite observations. *Environmental Research
509 Letters*, 17(3):034029, 2022.

- 510 [26] T. Zhong, N. Zhang, and M. Lv. A numerical study of the urban green roof and cool roof
511 strategies' effects on boundary layer meteorology and ozone air quality in a megacity.
512 *Atmospheric Environment*, 264:118702, 2021.